Chemical Science

EDGE ARTICLE

View Article Online
View Journal | View Issue

Check for updates

Cite this: Chem. Sci., 2020, 11, 6862

Self-activated Rh–Zr mixed oxide as a nonhazardous cocatalyst for photocatalytic hydrogen evolution†

Toshio Nishino,[a] Masaki Saruyama,*[b] Zhanzhao Li,[c] Yoshie Nagatsuma,[d] Mamiko Nakabayashi,[e] Naoya Shibata,[e] Taro Yamada,[d] Ryo Takahata,[b] Seiji Yamazoe,[f] Takashi Hisatomi,[g] Kazunari Domen[gh] and Toshiharu Teranishi*[b]

Received 6th March 2020
Accepted 18th June 2020

DOI: 10.1039/d0sc01363c

rsc.li/chemical-science

Efficient, robust and environmentally friendly cocatalysts for photocatalysts are important for large-scale solar hydrogen production. Herein, we demonstrate that a Rh–Zr mixed oxide is an efficient cocatalyst for hydrogen evolution. Impregnation of Zr and Rh precursors (Zr/Rh = 5 wt/wt%) formed $RhZrO_x$ cocatalyst particles on Al-doped $SrTiO_3$, which exhibited 31× higher photocatalytic water-splitting activity than a RhO_x cocatalyst. X-ray photoelectron spectroscopy proved that the dissociation of Cl^- ions from preformed Rh–Cl–Zr–O solid led to formation of the active phase of $RhZrO_x$, in which the Zr/Rh ratio was critical to high catalytic activity. Additional CoO_x loading as an oxygen evolution cocatalyst further improved the activity by 120%, resulting in an apparent quantum yield of 33 (±4)% at 365 nm and a long durability of 60 h. Our discovery could help scale up photocatalytic hydrogen production.

Introduction

Photocatalytic water-splitting is a promising technology for sustainable hydrogen production.[1,2] Various photocatalysts, such as TiO_2, $SrTiO_3$, TaON, GaN:ZnO, Ta_3N_5 and $Y_2Ti_2O_5S_2$, have been developed for effective utilization of solar energy.[3–8] Developing cocatalysts for photocatalysis is equally indispensable for improving photocatalytic activity;[9] this is because the cocatalysts promote extraction of excited charges from the photocatalysts and reduce the overpotential of the water-splitting reaction. Noble metals, particularly platinum group metals, are widely used for the hydrogen evolution reaction (HER); they reduce H_2O because of the metals' high activity and stability.[10] However, noble metals also catalyze backward reactions, such as O_2 photoreduction and H_2O formation, from evolved H_2 and O_2.[11] Suppressing the backward reactions is central for developing an efficient HER cocatalyst. Based on this concept, Pt@SiO_2 core@shell,[12] Rh@Cr_2O_3 core@shell[11,13] and Rh–Cr mixed oxide ($RhCrO_x$)[14] cocatalysts have been developed. In these systems, H_2O can access the noble metal surface, whereas oxygen access is prevented to dramatically suppress the backward reactions. Although both Rh@CrO_x and $RhCrO_x$ are commonly used because of their excellent activity, long-duration photo-irradiation causes dissolution of Cr^{6+} ions,[15] resulting in not only decreased catalytic activity but also environmental damage and health hazards. To meet increasing demands on solar-to-energy conversion, many scientists are trying to replace hazardous elements in solar active materials, as observed in organic–inorganic lead halide perovskite solar cells (*e.g.*, replace Pb with Sn or Bi).[16] Similarly, alternatives to Cr are necessary for large-scale, environmentally friendly photocatalytic water-splitting systems.[17]

In this paper, we demonstrate that a novel Rh–Zr mixed oxide ($RhZrO_x$) is an efficient HER cocatalyst for an Al-doped $SrTiO_3$ ($SrTiO_3$:Al) photocatalyst. $SrTiO_3$:Al is the best water-splitting photocatalyst under UV irradiation to date,[18] and can work in sunlight because of the high apparent quantum yield (AQY) in the UV region. Therefore, we chose $SrTiO_3$:Al synthesized by the flux-mediated method[15] as a model photocatalyst to explore new efficient cocatalysts. Surface characterizations of the cocatalysts using HRTEM, STEM-EDS and XPS indicate that the active $RhZrO_x$ phase forms by activation of the Rh–Cl–Zr–O mixed solid. A systematic study of loading conditions and

[a]Graduate School of Science and Technology, Nara Institute of Science and Technology, Ikoma, Nara, 630-0192, Japan

[b]Institute for Chemical Research, Kyoto University, Gokasho, Uji, Kyoto 611-0011, Japan. E-mail: saruyama@scl.kyoto-u.ac.jp; teranisi@scl.kyoto-u.ac.jp

[c]Department of Chemistry, Graduate School of Science, Kyoto University, Gokasho, Uji, Kyoto 611-0011, Japan

[d]Department of Chemical System Engineering, School of Engineering, The University of Tokyo, 7-3-1 Hongo, Bunkyo-ku, Tokyo 113-8656, Japan

[e]Institute for Engineering Innovation, The University of Tokyo, Hongo, Bunkyo-ku, Tokyo 113-8656, Japan

[f]Department of Chemistry, Graduate School of Science, Tokyo Metropolitan University, 1-1 Minami-Osawa, Hachioji, Tokyo 192-0397, Japan

[g]Research Initiative for Supra-Materials, Shinshu University, 4-17-1, Wakasato, Nagano, 380-8553, Japan

[h]Office of University Professor, The University of Tokyo, 7-3-1 Hongo, Bunkyo-ku, Tokyo 113-8656, Japan

† Electronic supplementary information (ESI) available: Experimental details, additional characterization and results. See DOI: 10.1039/d0sc01363c

electrocatalytic activity assessments of the cocatalyst uncovered the effect of Zr in the cocatalyst. Our novel, robust and nonhazardous Zr-based HER cocatalysts will be useful for large-scale solar hydrogen production.

Results and discussion

To find a new partner metal for Rh, we conducted element screening experiments (Fig. S1†). We chose impregnation to deposit cocatalysts on $SrTiO_3$:Al because impregnation is the easiest way to test a number of combinations without varying other experimental conditions. We fixed the weight ratio of metal to Rh (0.1 wt% *vs.* $SrTiO_3$:Al) at 5. Of 18 elements except for Cr, only five (Zr, Fe, Sm, La and Ce) showed higher activity than Rh alone. Among them, Zr exhibited outstanding H_2 evolution activity, 3.6× higher than the next most active element, Fe. The H_2/O_2 evolution molar ratio was approximately 2, indicating efficient overall water splitting. Zr is a nonhazardous element and its oxide is widely used in functional ceramics for bio-related applications. Therefore, Zr is a promising environmentally friendly alternative to Cr.

Then we optimized various parameters of $RhZrO_x$ cocatalysts on $SrTiO_3$:Al. We first varied the Zr/Rh weight ratio from 0 to 7 at a constant weight percent Rh of 0.1 wt% *vs.* $SrTiO_3$:Al (Fig. 1a). The catalytic activity increased in accordance with increasing Zr/Rh weight ratio from 0 to 5, and showed the highest H_2 evolution rate of 249 μmol h^{-1} at Zr/Rh = 5 wt/wt%, which is 31× higher than $RhO_x/SrTiO_3$:Al (Zr/Rh = 0). At Zr/Rh < 3 wt/wt%, the H_2 evolution rate drastically decreased after 1.5 h, indicating a Zr/Rh weight ratio >3 improves the catalyst's stability. Although the sample synthesized at Zr/Rh = 7 wt/wt% was stable, the overall activity was less than half (110 μmol h^{-1}) that at Zr/Rh = 5 wt/wt%. We also optimized the total quantity of cocatalyst at a fixed Zr/Rh weight ratio of 5 wt/wt% (Fig. 1b). When the loading quantity of cocatalyst was less than standard (Rh = 0.1 and Zr = 0.5 wt%), the H_2 evolution activity decreased considerably (22 μmol h^{-1}) because of the insufficient number of water reduction sites. However, loading a larger quantity of cocatalyst (Rh = 0.2 and Zr = 1.0 wt%) only slightly lessened the activity (221 μmol h^{-1}). Based on these results, the optimum quantity of cocatalyst for $SrTiO_3$:Al is Rh = 0.1 wt% and Zr = 0.5 wt%.

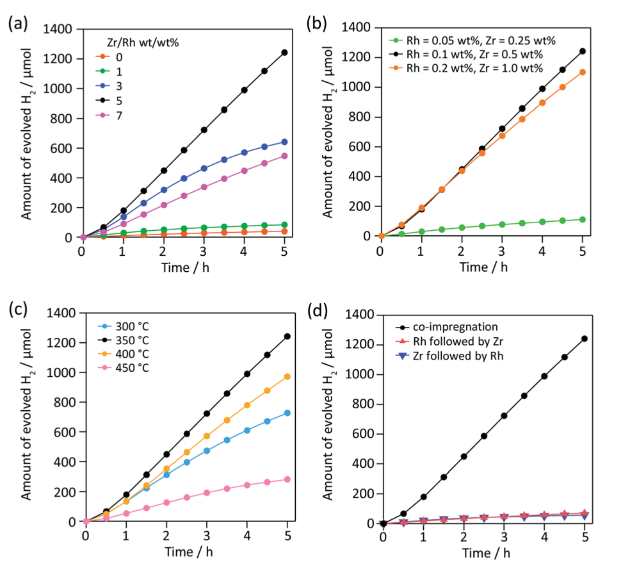

Fig. 1 Photocatalytic activities of $RhZrO_x/SrTiO_3$:Al synthesized in various experimental conditions. The quantity of evolved H_2 of $RhZrO_x/SrTiO_3$:Al synthesized (a) at various Zr/Rh weight ratios (Rh = 0.1 wt%), (b) at various quantities of Rh (Zr/Rh = 5 wt/wt%), (c) at various annealing temperatures (Rh = 0.1, Zr = 0.5 wt%) and (d) by co-impregnation and sequential impregnation (Rh = 0.1, Zr = 0.5 wt%). Reaction conditions: catalyst, 10 mg; solution, 20 mL of H_2O; light source, 300 W Xe lamp (λ = 300–450 nm).

Then we investigated the effect of calcination temperature in the range of 300–450 °C. $RhZrO_x/SrTiO_3$:Al calcined at 350 °C showed the highest H_2 evolution (Fig. 1c). A calcination temperature of 300 °C is too low to transform $ZrOCl_2 \cdot 8H_2O$ into ZrO_2 (Fig. S2 and Table S1†). The Cl/Zr molar ratio decreases with increasing the calcination temperature (Table S1†), indicating that higher calcination temperature assists the formation of ZrO_2. SEM images revealed that the cocatalyst size increased from several nanometres to hundreds of nanometres when we calcined the sample at a temperature higher than 400 °C, which decreased the number of active sites on the photocatalyst (Fig. S3†). The order of impregnation of two metal species is important, because the nanostructure of the cocatalyst affects the catalytic activity.[11] We compared a co-impregnated (Rh and Zr precursors mixed and loaded simultaneously) with sequentially impregnated (Rh and Zr precursors loaded sequentially) photocatalyst. The co-impregnated photocatalyst showed much higher activity than the sequentially impregnated photocatalyst (Fig. 1d), implying that the Rh–Zr mixed oxide was the active species for overall water splitting rather than the mixture of RhO_x and ZrO_x. Fig. S4† summarizes all aforementioned catalytic activities including O_2 evolution activity.

Next, we characterized the optimized $RhZrO_x$ cocatalysts on $SrTiO_3$:Al. We conducted HRTEM to observe the hetero-interface between $RhZrO_x$ and $SrTiO_3$:Al phases. We observed no appreciable spots in a FFT image from the cocatalyst region (light-blue square), whereas the $SrTiO_3$:Al region (orange square) exhibited spots that are attributable to crystalline $SrTiO_3$:Al (Fig. 2a), which indicates that the $RhZrO_x$ cocatalyst is amorphous. STEM-EDS elemental mapping analysis revealed that the elements Rh, Zr and O coexist in the cocatalysts and uniformly disperse on the photocatalysts (Fig. 2b).

For loading cocatalysts, we used $RhCl_3 \cdot 3H_2O$ and $ZrOCl_2 \cdot 8H_2O$ as Rh and Zr precursors, respectively. Considering the exceptional stability of anhydrous $RhCl_3$,[19] Cl may contaminate the Rh–Zr mixed oxide cocatalysts. At the impregnation conditions (350 °C for 1 h), $ZrOCl_2 \cdot 8H_2O$ was mostly converted into ZrO_2 (Fig. S2†), whereas $RhCl_3 \cdot 3H_2O$ released only H_2O to give anhydrous $RhCl_3$ (Fig. S5†), which is stable until 600 °C in air.[19] Thus Cl should exist in the $RhZrO_x$ cocatalyst; however, the XRD measurement for $RhZrO_x$ solid (Zr/Rh = 5 wt/wt%) did not indicate any metal chloride peaks (Fig. S6†). EDS analysis cannot indicate the coexistence of Rh and Cl, because the

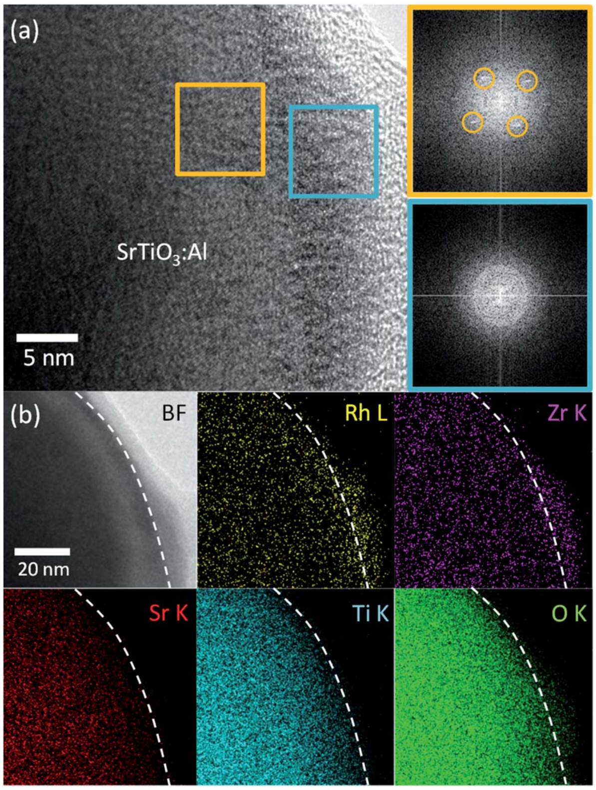

Fig. 2 Electron microscopy analyses of Rh–Zr oxide cocatalyst on $SrTiO_3$:Al. (a) HRTEM image and FFT images of $RhZrO_x/SrTiO_3$:Al at the interface. Outer bright layer: carbon-related contamination formed during observation. Orange and light-blue squares: $SrTiO_3$:Al and cocatalyst, respectively. (b) STEM-EDS elemental mapping images of $RhZrO_x/SrTiO_3$:Al at the interface. White broken lines: surface of $SrTiO_3$:Al.

characteristic X-ray energies from Rh-L and Cl-K largely overlap (2.6–2.9 keV). Therefore, we used XPS to confirm the presence of Cl in the cocatalyst, because the Rh 3d and Cl 2p peaks separately appear at approximately 310 and 198 eV, respectively. The XPS spectra of $RhZrO_x/SrTiO_3$:Al showed Cl 2p peaks along with Rh 3d and Zr 3d peaks (Fig. 3), indicating the presence of Cl in the cocatalyst. Rh 3d peaks have an intermediate feature between Rh_2O_3 and $RhCl_3\cdot3H_2O$, suggesting that the Rh is partially oxidized to a Rh–Cl–O species. Zr 3d and Cl 2p peaks can be assigned to Zr^{4+} of ZrO_2 and Cl^- of $RhCl_3\cdot3H_2O$, respectively. These results indicate the formation of Rh–Cl and Zr–O bonds. In addition, water-washed $RhZrO_x/SrTiO_3$:Al still has clear Cl 2p peaks along with Rh 3d and Zr 3d peaks, which is consistent with the intrinsic insolubility of anhydrous $RhCl_3$ in water. We also applied Ar bombardment to remove a several-nanometre surface extract of the samples to obtain the XPS spectra in the inner regions of the cocatalyst.[20] We detected three elements after Ar bombardment, indicating they were uniformly distributed in the cocatalyst. Thus, as-prepared cocatalyst can be described as a Rh–Cl–Zr–O solid. Because the Ar bombardment sometimes induces an XPS peak shift, we do not discuss the valence state of the elements in these experiments.

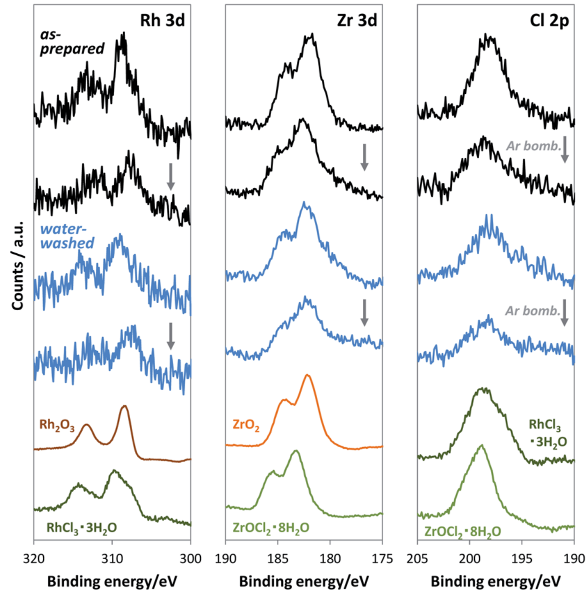

Fig. 3 XPS spectra of $RhZrO_x/SrTiO_3$:Al and reference materials at the energy ranges of (left) Rh 3d, (middle) Zr 3d and (right) Cl 2p. Black and blue spectra: as-prepared and water-washed samples, respectively, before and after Ar bombardment.

To understand why Rh–Cl–Zr–O solid-loaded $SrTiO_3$:Al exhibits high catalytic activity and durability, we investigated the structural change of Rh–Cl–Zr–O during the photocatalytic reaction. First, we examined the valence state of Rh during the photocatalytic reaction by *in situ* XANES measurements (Fig. S7†). We obtained XANES spectra every 11 min over the course of a 200 min photocatalytic reaction. The Rh K-edge spectra indicates that the valence of Rh retained nearly a trivalent state, which in turn indicates that the photo-excited electrons in $SrTiO_3$:Al do not reduce Rh^{3+} into Rh^0, as observed in previously reported $RhCrO_x$ cocatalysts.[21]

We conducted XPS measurements of $RhZrO_x/SrTiO_3$:Al after a 5 h reaction to further clarify the valence and composition

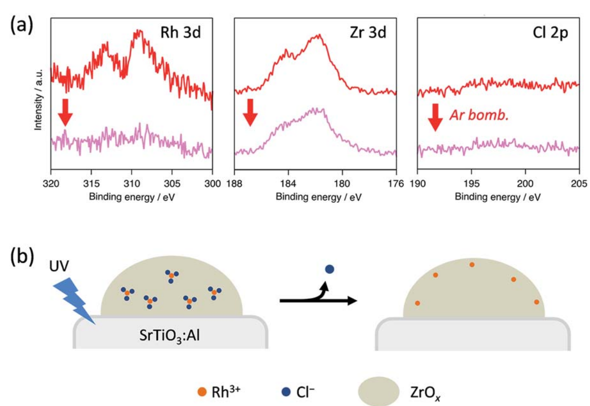

Fig. 4 (a) XPS spectra of Rh 3d, Zr 3d and Cl 2p peaks in a $RhZrO_x$ cocatalyst on $SrTiO_3$:Al after the reaction. (b) Schematic of the atomic rearrangement in Rh–Cl–Zr–O solid during photocatalysis.

changes of the elements in the cocatalyst (Fig. 4a). The Rh $3d_{5/2}$ peak at 309 eV showed no considerable shift after the reaction, which is consistent with our *in situ* XANES results. The Zr $3d_{5/2}$ peak at 182 eV was also unchanged after the reaction. However, the Cl 2p peak completely disappeared after the reaction, indicating the dissolution of Cl^- ions into the water during the reaction. Notably, the Rh 3d peak intensity considerably decreased after Ar bombardment, whereas the Zr 3d peak intensity remained unchanged. We did not observe the Cl 2p peak even inside the cocatalyst. ICP measurements revealed that the Zr/Rh weight ratio in the entire cocatalyst was retained after the reaction (Table S2†). These results strongly suggest that the Rh^{3+} ions are concentrated at the outer surface of the cocatalysts during the reaction without eluting into the water. This noteworthy concentration phenomenon does not result from the photoreduction of once-eluted Rh^{3+} on $SrTiO_3$:Al; this is because *in situ* XANES and XPS measurements revealed that Rh^{3+} was not reduced during the photocatalysis.

Considering the aforementioned results, we summarize the structural change of $RhZrO_x$ cocatalysts during photocatalysis as follows (Fig. 4b). Both Rh and Zr are uniformly dispersed in as-synthesized Rh–Cl–Zr–O solid in the forms of $RhCl_3$ and ZrO_2, respectively. As the reaction proceeds, the Cl^- ions move to the surface and elute to water. The Rh^{3+} ions also migrate together with Cl^- ions to the surface because of the strong Rh–Cl bond. As a result, the Rh^{3+} ions are condensed near the water/cocatalyst interface. However, the driving force for Cl^- dissolution remains to be clarified. In the resulting structure, the insulating ZrO_x layer may hinder the electron transfer from $SrTiO_3$:Al to Rh^{3+} reaction centres. Recently, it has been reported that the photoelectrodes coated with the insulating layers (ZrO_2, SiO_x, Al_2O_3, HfO_2, Ta_2O_5, *etc.*) exhibited enhanced photocatalytic activity, in which the photoexcited electrons can penetrate a few nanometre insulating overlayers.[22–26] Because our $RhZrO_x$ cocatalysts are several nanometres in size, it is reasonable that the photoexcited electrons can migrate through ZrO_x layers to reach Rh^{3+}.

The atom migration (induced by Cl^-) in the cocatalysts seems to affect the catalysts' catalytic properties. To confirm this migration effect, we synthesized $RhZrO_x/SrTiO_3$:Al catalysts from Cl-free precursors, such as $Rh(NO_3)_3\cdot xH_2O$ and $ZrO(NO_3)_2\cdot 2H_2O$, which were converted into mixed oxide cocatalysts through co-impregnation (Fig. S8†). The photocatalysts synthesized from $Rh(NO_3)_3\cdot xH_2O$ have considerably lower activity than those from $RhCl_3\cdot 3H_2O$ (Fig. S9†). Because the diameters of the cocatalysts were similar regardless of the precursors, a morphological effect on the activity can be excluded (Fig. S10†). These results strongly suggest that Cl^- elution from the Rh–Cl–Zr–O solid formed the $RhZrO_x$ active species with the optimal spatial distribution of Rh, Zr and O for the overall water-splitting reaction.

The ZrO_x-loaded $SrTiO_3$:Al showed almost no H_2 evolution activity (1 μmol h^{-1}), therefore, the ZrO_x does not function as a HER-active centre (Fig. S11†). To understand how Zr contributes to the activity enhancement, we conducted electrochemical catalysis measurements of $RhZrO_x$. We loaded the $RhZrO_x$ cocatalysts on carbon powder (XC-72) by the same impregnation method adopted for $SrTiO_3$:Al. We evaluated the catalytic activity of the backward reaction by measuring the current density of the oxygen reduction reaction (ORR) in O_2-saturated 1 M aqueous Na_2SO_4. Linear sweep voltammograms showed that the onset potential for the ORR shifted in the negative direction, and the current density at 0.4 V *vs.* reversible hydrogen electrode decreased from 2.5 to 1.3 mA cm^{-2} as the Zr/Rh weight ratio increased from 0 to 7 (Fig. S13a and b†). This indicates that increasing the Zr/Rh weight ratio suppresses the ORR. We also evaluated the HER activity from an overpotential for the water reduction reaction in Ar-saturated 1 M aqueous Na_2SO_4. Overpotential of HER at −8 mA cm^{-2} increased from 445 to 524 mV in accordance with increasing Zr/Rh weight ratio (Fig. S13c and d†), which suggests that the larger quantity of Zr also suppresses the water reduction activity. This tendency accounts for the reason why Zr/Rh = 5 wt/wt% showed the highest water-splitting activity; that is, at Zr/Rh = 0–5 wt/wt%, suppression of the backward reaction is the main contributor to the improvement of the catalytic activity. In the range of Zr/Rh > 5 wt/wt%, deactivation of HER exceeds the suppression of the backward reaction.

From the structural point of view, we have to mention that it is hard to clarify whether the structure of $RhZrO_x$ on XC-72 is exactly the same as that of activated $RhZrO_x$ on $SrTiO_3$:Al, because the amount of $RhZrO_x$ used in the electrochemical test was not enough for XPS measurement (Rh + Zr = 0.12 μg). Although the Cl^- effect is unclear in electrochemical catalyses without structural characterization, the $RhZrO_x$/XC-72 prepared from $Rh(NO_3)_3\cdot xH_2O$ showed different ORR and HER activities from that prepared from $RhCl_3\cdot 3H_2O$ (Fig. S13b and d†). One clear trend is that both ORR and HER activities decrease with increasing the Zr/Rh weight ratio for each catalyst (Fig. S13b and d†), which suggests that the addition of ZrO_x hinders both ORR and HER of Rh^{3+} regardless of the Cl^--mediated activation.

The ORR blocking ability of ZrO_x was confirmed in the photocatalysis of $RhZrO_x/SrTiO_3$:Al (Zr/Rh = 5 wt/wt%) by monitoring the concentrations of accumulated H_2 and O_2 in a reaction vessel after turning off the light irradiation (Fig. S14†). H_2 and O_2 concentrations in the reactor remained almost unchanged (>95%) over the subsequent 9 h in the dark, indicating that the backward reaction was strongly suppressed on $RhZrO_x/SrTiO_3$:Al with Zr/Rh = 5 wt/wt%. This result also suggests that the ratio of Zr/Rh = 5 wt/wt% is sufficient to suppress the backward reaction, which is qualitatively linked to the less ORR activity of $RhZrO_x$ cocatalyst with Zr/Rh = 5 wt/wt% in electrochemical results (Fig. S13a†). Additionally, this result also supports the conclusion that the less activity of $RhZrO_x/SrTiO_3$:Al with Zr/Rh = 7 wt/wt% results from the decreased HER activity, as shown in Fig. S13c.†

Co-loading of both HER and oxygen evolution reaction (OER) cocatalysts synergistically enhances the photocatalytic overall water splitting.[27] For example, co-loading of cobalt oxide (CoO_x) with $RhCrO_x$ on $SrTiO_3$:Al enhances both the catalytic activity and durability.[15] Encouraged by these results, we co-loaded CoO_x and $RhZrO_x$ on $SrTiO_3$:Al (CoO_x + $RhZrO_x/SrTiO_3$:Al) by sequential impregnation. Initially, we loaded CoO_x (Co = 0.1 wt% *vs.* $SrTiO_3$:Al) on $SrTiO_3$:Al, followed by loading $RhZrO_x$

(Rh = 0.1 and Zr = 0.5 wt% *vs.* $SrTiO_3$:Al). The HER activity of CoO_x + $RhZrO_x/SrTiO_3$:Al was 296 μmol h^{-1}, which is 1.2× higher than that of $RhZrO_x/SrTiO_3$:Al (Fig. 5a). We confirmed that 0.1 wt% *vs.* $SrTiO_3$:Al is an optimum amount of Co in the range of 0.05–0.2 wt% (Fig. S15†). Other well-known OER cocatalysts like NiO_x and IrO_x were also tested as additives on $RhZrO_x/SrTiO_3$:Al but their activities did not exceed the CoO_x + $RhZrO_x/SrTiO_3$:Al (Fig. S16†). We calculated the AQY of CoO_x + $RhZrO_x/SrTiO_3$:Al to be 33 (±4)% at 365 nm. The solar-to-hydrogen efficiency (STH) was estimated to be 0.21% (Fig. S17†). The stability was also improved by co-loading CoO_x with $RhZrO_x$ (Fig. 5b). Because $CoO_x/SrTiO_3$:Al showed much lower activity for HER (Fig. 5a and b), we conclude that coexistence of CoO_x and $RhZrO_x$ has a synergetic effect on the catalytic activity. In the case of the CoO_x + $RhCrO_x$ combination, CoO_x promotes hole extraction from $SrTiO_3$:Al, which disrupts hole migration to $RhCrO_x$ to suppress the degradation,[21] and also catalyzes water oxidation. We consider that this positive effect would also be effective for $RhZrO_x/SrTiO_3$:Al. A 60 h long-term stability test in 10 h intervals revealed that the gas evolution rate was relatively constant to the end of the reaction, maintaining a H_2/O_2 molar ratio of approximately 2 (Fig. 5c and d), indicating the robustness of CoO_x + $RhZrO_x/SrTiO_3$:Al.

Although we have shown the superior catalytic performance of $RhZrO_x/SrTiO_3$:Al, the activity is still less than that of $RhCrO_x/SrTiO_3$:Al, which has a >50% AQY at 365 nm (Table S3†).[15] In the Rh@Cr_2O_3 cocatalyst, the Cr_2O_3 layer suppresses only the ORR and does not hinder the HER of Rh.[11] This seems to be one of the reasons why $RhZrO_x/SrTiO_3$:Al has less activity than $RhCrO_x/SrTiO_3$:Al. To enhance the activity of $RhZrO_x/SrTiO_3$:Al, doping foreign metals into ZrO_2 may increase proton conductivity.[28] This strategy may help proton penetration towards the Rh reaction centres to evolve a larger quantity of H_2. Robot-operating combinatorial experiments will help researchers discover such novel ternary or quaternary oxides cocatalyst materials from enormous numbers of candidates.[29]

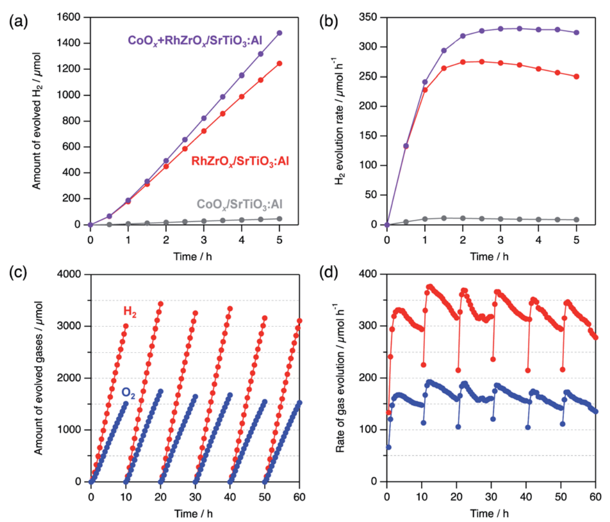

Fig. 5 (a) Quantity of evolved H_2 and (b) H_2 evolution rate of CoO_x + $RhZrO_x/SrTiO_3$:Al, $RhZrO_x/SrTiO_3$:Al and $CoO_x/SrTiO_3$:Al. (c) Quantity of evolved gases and (d) evolution rate of gases of CoO_x + $RhZrO_x/SrTiO_3$:Al in a long-term test for 60 h. Red and blue circles represent H_2 and O_2, respectively. Reaction conditions: catalyst, 10 mg; solution, 20 mL of H_2O; light source, 300 W Xe lamp (λ = 300–450 nm).

Conclusions

We demonstrated that a Rh–Zr mixed oxide efficiently functions as a HER cocatalyst on $SrTiO_3$:Al. The active phase for HER, $RhZrO_x$, formed by spontaneous Cl-dissolution-assisted activation of the Rh–Cl–Zr–O solid solution. Unexpected Cl^- contamination was found to sacrificially assist the formation of suitable spatial distributions of Rh^{3+} and Zr^{4+} in $RhZrO_x$ cocatalyst during photocatalysis. Electrochemical measurements showed that addition of Zr suppresses not only the ORR, but also the HER of Rh. We used this fact to determine the proper weight ratio of Zr/Rh (=5) for overall water splitting. Additional deposition of an OER cocatalyst, CoO_x, further improved the photocatalytic activity and stability of $RhZrO_x/SrTiO_3$:Al. Our nonhazardous Zr-based cocatalyst will be useful for large-scale applications to photocatalytic water splitting.

Conflicts of interest

There are no conflicts to declare.

Acknowledgements

We thank H. Tokudome and S. Okunaka of TOTO Ltd. for preparing $SrTiO_3$:Al. This work was partly supported by the Artificial Photosynthesis Project of the New Energy and Industrial Technology Development Organization (NEDO) of Japan and JSPS KAKENHI for Scientific Research S (Grant No. JP19H0563) (T. T.), and Young Scientists B (Grant No. 17K14081) (M. S.).

References

1 B. A. Pinaud, J. D. Benck, L. C. Seitz, A. J. Forman, Z. Chen, T. G. Deutsch, B. D. James, K. N. Baum, G. N. Baum, S. Ardo, H. Wang, E. Miller and T. F. Jaramillo, *Energy Environ. Sci.*, 2013, **6**, 1983.
2 A. Kudo and Y. Miseki, *Chem. Soc. Rev.*, 2009, **38**, 253.
3 S. Sato and J. M. White, *Chem. Phys. Lett.*, 1980, **72**, 83.
4 Y. Sasaki, H. Kato and A. Kudo, *J. Am. Chem. Soc.*, 2013, **135**, 5441.
5 K. Maeda, M. Higashi, D. Lu, R. Abe and K. Domen, *J. Am. Chem. Soc.*, 2010, **132**, 5858.
6 K. Maeda, K. Teramura, D. Lu, T. Takata, N. Saito, Y. Inoue and K. Domen, *Nature*, 2006, **440**, 295.
7 Z. Wang, Y. Inoue, T. Hisatomi, R. Ishikawa, Q. Wang, T. Takata, S. Chen, N. Shibata, Y. Ikuhara and K. Domen, *Nat. Catal.*, 2018, **1**, 756.
8 Q. Wang, M. Nakabayashi, T. Hisatomi, S. Sun, S. Akiyama, Z. Wang, Z. Pan, X. Xiao, T. Watanabe, T. Yamada, N. Shibata, T. Takata and K. Domen, *Nat. Mater.*, 2019, **18**, 827.
9 K. Takanabe, *ACS Catal.*, 2017, **7**, 8006.

10 M. Yoshida, A. Yamakata, K. Takanabe, J. Kubota, M. Osawa and K. Domen, *J. Am. Chem. Soc.*, 2009, **131**, 13218.
11 M. Yoshida, K. Takanabe, K. Maeda, A. Ishikawa, J. Kubota, Y. Sakata, Y. Ikezawa and K. Domen, *J. Phys. Chem. C*, 2009, **113**, 10151.
12 J. A. Bau and K. Takanabe, *ACS Catal.*, 2017, **7**(11), 7931.
13 T. Ikeda, A. Xiong, T. Yoshinaga, K. Maeda, K. Domen and T. Teranishi, *J. Phys. Chem. C*, 2013, **117**, 2467.
14 K. Maeda, K. Teramura, D. Lu, T. Takata, N. Saito, Y. Inoue and K. Domen, *J. Phys. Chem. B*, 2006, **110**, 13753.
15 H. Lyu, T. Hisatomi, Y. Goto, M. Yoshida, T. Higashi, M. Katayama, T. Takata, T. Minegishi, H. Nishiyama, T. Yamada, Y. Sakata, K. Asakura and K. Domen, *Chem. Sci.*, 2019, **10**, 3196.
16 F. Giustino and H. J. Snaith, *ACS Energy Lett.*, 2016, **1**, 1233.
17 A. T. Garcia-Esparza, T. Shinagawa, S. Ould-Chikh, M. Qureshi, X. Peng, N. Wei, D. H. Anjum, A. Clo, T. C. Weng, D. Nordlund, D. Sokaras, J. Kubota, K. Domen and K. Takanabe, *Angew. Chem., Int. Ed.*, 2017, **56**, 5780.
18 T. Takata and K. Domen, *J. Phys. Chem. C*, 2009, **113**, 19386.
19 W. Balcerowiak, *J. Therm. Anal. Calorim.*, 2003, **71**, 559.
20 S. P. Phivilay, C. A. Roberts, A. D. Gamalski, E. A. StachShiran, Z. Luan, N. Y. Tang, A. Xiong, A. A. Puretzky, F. F. Tao, K. Domen and I. E. Wachs, *ACS Catal.*, 2018, **8**, 6650.
21 K. Maeda, K. Teramura, H. Masuda, T. Takata, N. Saito, Y. Inoue and K. Domen, *J. Phys. Chem. B*, 2006, **110**, 13107.
22 J. Liu, T. Hisatomi, D. H. K. Murthy, M. Zhong, M. Nakabayashi, T. Higashi, Y. Suzuki, H. Matsuzaki, K. Seki, A. Furube, N. Shibata, M. Katayama, T. Minegishi and K. Domen, *J. Phys. Chem. Lett.*, 2017, **8**, 375.
23 S. Y. Lim, D. Han, Y. R. Kim and T. D. Chung, *ACS Appl. Mater. Interfaces*, 2017, **9**, 23698.
24 R. Fan, J. Mao, Z. Yin, J. Jie, W. Dong, L. Fang, F. Zheng and M. Shen, *ACS Appl. Mater. Interfaces*, 2017, **9**, 6123.
25 J. Quinn, J. Hemmerling and S. Linic, *ACS Energy Lett.*, 2019, **4**, 2632.
26 T. Wang, S. Liu, H. Li, C. Li, Z. Liu and J. Gong, *Ind. Eng. Chem. Res.*, 2019, **58**, 5510.
27 K. Maeda, A. Xiong, T. Yoshinaga, T. Ikeda, N. Sakamoto, T. Hisatomi, M. Takashima, D. Lu, M. Kanehara, T. Setoyama, T. Teranishi and K. Domen, *Angew. Chem., Int. Ed.*, 2010, **49**, 4096.
28 J. A. Dawson and I. Tanaka, *Langmuir*, 2014, **30**, 10456.
29 R. Saito, Y. Miseki, W. Nini and K. Sayama, *ACS Comb. Sci.*, 2015, **17**, 592.

